Article

Size-Induced Enhancement of Chemical Exchange Saturation Transfer (CEST) Contrast in Liposomes

Jason M. Zhao, Yah-el Har-el, Michael T. McMahon, Jinyuan Zhou, A. Dean Sherry, George Sgouros, Jeff W. M. Bulte, and Peter C. M. van Zijl

J. Am. Chem. Soc., **2008**, 130 (15), 5178-5184 • DOI: 10.1021/ja710159q • Publication Date (Web): 25 March 2008

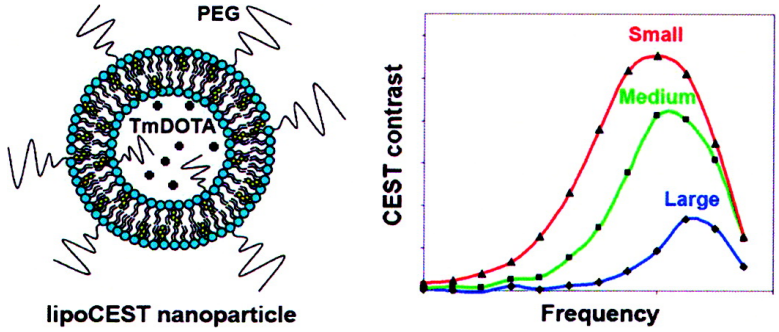

More About This Article

Additional resources and features associated with this article are available within the HTML version:

- Supporting Information
- Access to high resolution figures
- Links to articles and content related to this article
- Copyright permission to reproduce figures and/or text from this article

View the Full Text HTML

J|A|C|S
ARTICLES

Published on Web 03/25/2008

Size-Induced Enhancement of Chemical Exchange Saturation Transfer (CEST) Contrast in Liposomes

Jason M. Zhao,*[,†,§] Yah-el Har-el,[†] Michael T. McMahon,[†,§] Jinyuan Zhou,[†,§] A. Dean Sherry,[‡] George Sgouros,[†] Jeff W. M. Bulte,[†,&,#] and Peter C. M. van Zijl*[,†,§]

Russell H. Morgan Department of Radiology and Radiological Science, Johns Hopkins University School of Medicine, F.M. Kirby Research Center for Functional Brain Imaging, Kennedy Krieger Institute, Department of Chemical and Biomolecular Engineering, Johns Hopkins University Whiting School of Engineering, Cellular Imaging Section and Vascular Biology Program, Institute for Cell Engineering, Johns Hopkins University School of Medicine, Baltimore, Maryland 21205, and Advanced Imaging Research Center, University of Texas Southwestern Medical Center, Dallas, Texas 75390

Received November 8, 2007; E-mail: jmzhao@mri.jhu.edu; pvanzijl@jhu.edu

Abstract: Liposome-based chemical exchange saturation transfer (lipoCEST) agents have shown great sensitivity and potential for molecular magnetic resonance imaging (MRI). Here we demonstrate that the size of liposomes can be exploited to enhance the lipoCEST contrast. A concise analytical model is developed to describe the contrast dependence on size for an ensemble of liposomes. The model attributes the increased lipoCEST contrast in smaller liposomes to their larger surface-to-volume ratio, causing an increased membrane water exchange rate. Experimentally measured rates correlate with size, in agreement with the model. The water permeability of liposomal membrane is found to be 1.11 ± 0.14 μm/s for the specific lipid composition at 22 °C. Availability of the model allows rational design of the size of liposomes and quantification of their properties. These new theoretical and experimental tools are expected to benefit applications of liposomes to sensing the cellular environment, targeting and imaging biological processes, and optimizing drug delivery properties.

I. Introduction

Molecular magnetic resonance imaging (MRI) is an emerging field that has the goal of combining the high spatial resolution of MRI with the high specificity of molecular targeting.[1,2] One important limitation of applying MRI to molecular imaging lies in its inherent low sensitivity compared to nuclear medicine or optical methods such as fluorescence. To overcome this barrier, new agents are continuously being developed that have better relaxation properties or a high payload of contrast materials.[3] For example, T_1-based gadolinium (Gd) contrast agents have been heavily investigated due to their clinical translational values. Macromolecular carriers such as linear polymers[4] and dendrimers[5,6] can have hundreds or even thousands of Gd chelates covalently linked together, greatly enhancing the relaxation effects of these contrast agents on a per Gd basis. Nanoparticle carriers have also been shown to enhance sensitivity: Tilcock and Unger et al. encapsulated ~100 mM of Gd-DTPA in liposomes to create T_1 images of hepatic metastasis in rats.[7,8]

Conventionally, molecular MRI contrast has been based on the shortening of the relaxation times, T_1, T_2, or T_2*, using paramagnetic complexes. By contrast, chemical exchange saturation transfer (CEST) is a relatively recent technique[9] that involves the physical transfer of saturated exchangeable protons from a contrast agent to the surrounding water, resulting in a reduction of the water signal. If this transfer rate is high or if there are many saturated protons on the contrast agent, CEST can efficiently reduce the water signal in a matter of seconds and detect the presence of micromolar concentrations of the contrast agent. CEST research started with small diamagnetic molecules (DIACEST) such as sugars and amino acids[10,11] and

† Russell H. Morgan Department of Radiology and Radiological Science, Johns Hopkins University School of Medicine.
§ Kennedy Krieger Institute.
& Johns Hopkins University Whiting School of Engineering.
‡ University of Texas Southwestern Medical Center.
# Institute for Cell Engineering, Johns Hopkins University School of Medicine.

(1) Weissleder, R.; Mahmood, U. *Radiology* **2001**, *219*, 316–333.
(2) Glunde, K.; Pathak, A. P.; Bhujwalla, Z. M. *Trends Mol. Med.* **2007**, *13*, 287–297.
(3) Aime, S.; Crich, S. G.; Gianolio, E.; Giovenzana, G. B.; Tei, L.; Terreno, E. *Coord. Chem. Rev.* **2006**, *250*, 1562.
(4) Casali, C.; Janier, M.; Canet, E.; Obadia, J. F.; Benderbous, S.; Corot, C.; Revel, D. *Acad. Radiol.* **1998**, *5*, S214–S218.
(5) Bryant, L. H.; Brechbiel, M. W.; Wu, C.; Bulte, J. W. M.; Herynek, V.; Frank, J. A. *J. Magn. Reson.* **1999**, *9*, 348–352.
(6) Kobayashi, H.; Brechbiel, M. W. *Adv. Drug Delivery Rev.* **2005**, *57*, 2271–2286.
(7) Tilcock, C.; Unger, E.; Cullis, P.; MacDougall, P. *Radiology* **1989**, *171*, 77–80.
(8) Unger, E.; Winokur, T.; MacDougall, P.; Rosenblum, J.; Clair, M.; Gatenby, R.; Tilcock, C. *Radiology* **1989**, *171*, 81–85.
(9) Zhou, J.; van Zijl, P. C. *Progr. NMR Spectrosc.* **2006**, *48*, 109–136.
(10) Wolff, S. D.; Balaban, R. S. *J. Magn. Reson.* **1990**, *86*, 164–169.
(11) Ward, K. M.; Aletras, A. H.; Balaban, R. S. *J. Magn. Reson.* **2000**, *143*, 79–87.

 10.1021/ja710159q CCC: $40.75

quickly evolved into macromolecular polypeptides[12] and oligonucleotides[13] and a class of paramagnetic lanthanide agents (PARACEST).[14–17] More recently, Aime et al. designed a CEST nanoparticle system by encapsulating paramagnetic shift agents inside liposomes (lipoCEST),[18] thereby shifting the resonant frequency of the intraliposomal water relative to the bulk water. When selectively labeling intraliposomal water through application of a radiofrequency (RF) presaturation pulse, the MR saturation is transferred via the chemical exchange of water across the liposomal membrane. The authors reported great MR sensitivities using liposome concentrations as low as 90 pM. This approach was further improved by shrinking liposomes into a nonspherical shape by exposing them under hypertonic conditions, thus further shifting the resonance frequency of intraliposomal water away from bulk water via the bulk magnetic susceptibility effect.[19] Furthermore, Aime et al. encapsulated a gadolinium T_1 agent inside shrunken liposomes and found that the nanoparticles exhibit not only good T_1 and T_2 relaxivities but also good CEST contrast, thus creating the first versatile agent with T_1, T_2, and CEST capabilities all in one package.[20]

Liposomes as delivery vehicles for CEST agents present a great potential for MRI and therapy because they are biocompatible and well-established as a drug delivery platform that can easily be translated into the clinic. Here we expand on previous studies to elucidate the mechanism underlying the lipoCEST effect. We present a concise analytical model to describe the contrast dependence on size for an ensemble of liposomes. Size-dependent measurements illustrate that smaller liposomes can generate increased lipoCEST contrast.

II. Theory

For a single liposome of radius r_l, surface area S_l, volume V_l, and membrane permeability P_l, the water exchange rate from intra- to extraliposomal space (k_{lw}) is related to its permeability surface area product by

$$P_l S_l = k_{lw} V_l \text{ or } k_{lw} = 3P_l/r_l \tag{1}$$

For a system of N_l liposomes with a distribution of sizes, the exchange equilibrium condition implies that

$$P_l \sum_{i=1}^{N_l} S_{l,i} = \sum_{i=1}^{N_l} k_{lw,i} V_{l,i} = \overline{k_{lw}} V_l = k_{wl} V_w \tag{2}$$

where V_l and V_w denote the total intra- and extraliposomal water volumes; k_{wl} is the extra- to intraliposomal water exchange rate. Equation 2 implies that the two exchange rates of a dilute solution of liposomes are related by the intraliposomal water fraction, $x_l = V_l/(V_l + V_w) \approx V_l/V_w$; more precisely

$$k_{wl} = \overline{k_{lw}} V_l / V_w = \overline{k_{lw}} x_l \tag{3}$$

Using eq 2, k_{wl} can be rewritten in terms of the liposomal molar concentration $[l]$

$$k_{wl} = P_l \sum_{i=1}^{N_l} S_{l,i}/V_w = P_l N_A [l] \sum_{r=0}^{\infty} f(r) \cdot 4\pi r^2 \tag{4}$$

where $f(r)$ is the fraction of liposomes with radius r, and N_A is Avogadro's number. Thus the exchange rate is directly proportional to the membrane permeability and the total membrane surface area.

When a liposome encapsulates a shift agent in the liposomal lumen, the magnetic susceptibilities and thus the resonance frequencies of the water inside and outside differ. The membrane water exchange rate can be measured from the magnetization transfer by selectively irradiating at the frequency offset ($\Delta\omega$) of the intraliposomal water with respect to bulk water and observing the disappearance of bulk water signal as a function of the irradiating time. The efficiency of the proton transfer process for a CEST agent is commonly expressed as the proton transfer ratio (PTR). The analytical solution for PTR depends on two assumptions: (i) frequency matching between the RF presaturation pulse and the intraliposomal water, and (ii) a large spectral separation between the intraliposomal and bulk water frequencies. Under these two assumptions, the time-dependent PTR following a RF pulse duration of T_{sat} is[21]

$$\mathrm{PTR}(T_{sat}) = 1 - \frac{M_{sat}(T_{sat})}{M_{0w}} = \frac{k_{wl}\alpha}{r_{1w}}[1 - \exp(-r_{1w} \cdot T_{sat})] \tag{5}$$

where $r_{1w} = R_{1w} + k_{wl}$ is the effective relaxation rate. R_{1w} represents the longitudinal relaxation of water in the presence of paramagnetic agents and can be calculated from the agent-free relaxation rate ($R_{1w,0}$) and the exchange rate[22]

$$R_{1w} = R_{1w,0} + \frac{1}{1/(x_l R_l) + 1/k_{wl}} \tag{6}$$

The saturation efficiency α is determined by the power of the RF pulse and the exchange and relaxation rates of water protons:

$$\alpha = \omega_1^2/(\omega_1^2 + pq) \tag{7}$$

where ω_1 is the power of the RF pulse, $p = r_{2l} - k_{lw}k_{wl}/r_{2w}$ and $q = r_{1l} - k_{lw}k_{wl}/r_{1w}$, with $r_{1l} = R_{1l} + k_{lw}$, $r_{2l} = R_{2l} + k_{lw}$ and $r_{2w} = R_{2w} + k_{wl}$. Since R_{2w} in a dilute liposome sample does not affect the PTR as significantly as R_{1w}, as a good approximation, the transverse relaxation rate of water without liposomes can be used.

Equation 5 suggests that the dynamics of PTR is dictated by the rate constant r_{1w}, that is, the larger the r_{1w}, the faster for PTR to reach its steady-state value. The permeability of the membrane can then be calculated from eq 4, with the knowledge of k_{wl} from the time-dependent PTR experiment, the surface area of liposomes from their size distribution, and the concentration from fluorescence measurements (Experimental Section).

(12) Goffeney, N.; Bulte, J. W. M.; Duyn, J.; Bryant, L. H.; van Zijl, P. C. M. *J. Am. Chem. Soc.* **2001**, *123*, 8628.
(13) Snoussi, K.; Bulte, J. W. M.; Gueron, M.; van Zijl, P. C. M. *Magn. Reson. Med.* **2003**, *49*, 998–1005.
(14) Zhang, S.; Merritt, M.; Woessner, D. E.; Lenkinski, R.; Sherry, A. D. *Acc. Chem. Res.* **2003**, *36*, 783.
(15) Aime, S.; Cabella, C.; Colombatto, S.; Geninatti Crich, S.; Gianolio, E.; Maggioni, F. *J. Magn. Reson.* **2002**, *16*, 394–406.
(16) Vinogradov, E.; He, H.; Lubag, A.; Balschi, J. A.; Sherry, A. D.; Lenkinski, R. E. *Magn. Reson. Med.* **2007**, *58*, 650.
(17) Liu, G.; Li, Y.; Pagel, M. D. *Magn. Reson. Med.* **2007**, *58*, 1249–1256.
(18) Aime, S.; Delli Castelli, D.; Terreno, E. *Angew. Chem., Int. Ed.* **2005**, *44*, 5513–5515.
(19) Terreno, E.; Cabella, C.; Carrera, C.; Castelli, D. D.; Mazzon, R.; Rollet, S.; Stancanello, J.; Visigalli, M.; Aime, S. *Angew. Chem., Int. Ed.* **2006**, *45*, 1–4.
(20) Aime, S.; Castelli, D. D.; Lawson, D.; Terreno, E. *J. Am. Chem. Soc.* **2007**, *129*, 2430–2431.
(21) Zhou, J.; Wilson, D. A.; Sun, P. Z.; Klaus, J. A.; van Zijl, P. C. M. *Magn. Reson. Med.* **2004**, *51*, 945–952.
(22) Koenig, S. H.; Ahkong, Q. F.; Brown, R. D.; Lafleur, M.; Spiller, M.; Unger, E.; Tilcock, C. *Magn. Reson. Med.* **1992**, *23*, 275–286.

III. Experimental Section

1. Preparation of TmDOTA and Liposomes. Thulium 1,4,7,10-tetraaza-1,4,7,10-tetrakis(carboxymethyl)cyclododecane (TmDOTA) was synthesized by the complexation of DOTA with $Tm(OH)_3$.[23] $TmCl_3$ (Sigma-Aldrich, Milwaukee, WI) was converted to $Tm(OH)_3$ by adding 3 equiv of NaOH in water. The solid formed was washed with water until the pH decreased to 8. DOTA was added to the suspension of $Tm(OH)_3$ in water, and the solution was stirred overnight with the pH at 6. The solution was then heated to 60 °C for 24 h to ensure complete complexation. The solution was lyophilized, and a small amount (50 mg) of the powder was used for an inductively coupled plasma (ICP) analysis to determine the %Tm (w/w) = 22.5%. From the MW of Tm (168.93), the MW of the TmDOTA complex was determined to be 750.8 g/mol.

The liposome preparation followed a method reported previously.[24] All lipids were purchased from Avanti Polar Lipids (Alabaster, AL). We mixed phosphatidylcholine (PC) and cholesterol in a 1:1 molar ratio with 0.5 mol % L-α-phosphatidylethanolamine-*N*-lissamine rhodamine-B-sulfonyl (Rd-PE) and 3 mol % 1,2-dimyristoyl-*sn*-glycero-3-phosphoethanolamine-*N*-[methoxy-(polyethylene glycol)-2000] (PEG-PE) in $CHCl_3$, then dried them in a rotary evaporator. For passive contrast agent entrapment, lipids were resuspended in phosphate buffer solution (PBS) containing 200 mM TmDOTA. The suspension was then annealed at 55 °C for 2 h. To form unilamellar vesicles, the lipid suspension was subsequently taken through 21 cycles of extrusion through doubly stacked polycarbonate filters with 50, 400, or 800 nm pore sizes. Unentrapped TmDOTA was removed by a size exclusion column (Sephadex G-50) and eluted with PBS.

2. Characterization of Liposome Concentrations and Sizes. Liposome concentrations were quantified by measuring the Rd-PE fluorescence with a fluorescence plate reader (PerkinElmer, Waltham, MA). A fluorescence versus Rd-PE concentration calibration curve was obtained by measuring the fluorescence of the known Rd-PE containing lipid solution at five different dilutions. On the basis of this calibration, the final Rd-PE concentration of the liposomes, [RdPE], was determined. The liposome molar concentration, [*l*], was calculated from the molar fraction of Rd-PE (F_{RdPE}) and the size distribution of liposomes as follows:

$$[l] = \frac{[\mathrm{RdPE}]/F_{\mathrm{RdPE}}}{4\pi\langle r_l^2\rangle/A + 4\pi\langle (r_l - t)^2\rangle/A} \tag{8}$$

where r_l is the hydrodynamic radii of liposomes (i.e., from the center to the outer surface of membrane), $t = 5$ nm is the average membrane thickness, $A = 0.445$ nm^2 is the average area of the lipid headgroup, and <> denotes ensemble averages calculated from size distributions. The intraliposomal water fraction can also be calculated

$$x_l = \frac{4\pi\langle (r-t)^3\rangle N_l}{3V} = \frac{4\pi}{3} N_{\mathrm{A}}[l]\langle (r-t)^3\rangle \tag{9}$$

where N_l is the total number of liposomes and $V = V_l + V_w$ is the total volume.

The hydrodynamic size distributions of the liposomes were measured using dynamic light scattering (DLS, Malvern Nanosizer ZS90, Worcestershire, UK) with a 633 nm He−Ne laser light source. DLS measures the scattered laser intensity fluctuations from liposomes and calculates the distribution of liposome sizes from the autocorrelation function of the fluctuations. All DLS parameters were calculated using the manufacturer's software. The samples were prepared by diluting 20–50 μL of liposomes in 1 mL of PBS and were measured three times using the DLS instrument (Supporting Information).

3. MR Protocols. All MR experiments were performed on a triple-axis gradient 11.7T Bruker Avance system at a room temperature of 22 ± 1 °C. The spectroscopy experiments used the high-resolution NMR probe, while the imaging experiments used the Bruker 15 mm volume probe and the Micro5 gradient coil. The liposome samples were placed in standard 5 mm NMR tubes, and 5% (v/v) D_2O was added to each tube for locking. The magnet was shimmed by gradient shimming, and further improvement was achieved by manual shimming. Radiation damping is an issue when studying water at high magnetic fields. We did not detune the probe during all the PTR measurements to avoid previously reported artifacts,[25] instead small gradients were applied to dephase transverse magnetization during the evolution periods in the spin–echo sequence.[26]

NMR spectra were Fourier transformed, zero-order phase and baseline corrected on the Bruker console using Xwinnmr. PTR measurements were performed using the standard spin–echo sequence with a presaturation block RF pulse of duration T_{sat}. The offset frequencies ranged from 0.25 to 3.25 ppm with a 0.25 ppm stepsize after centering the bulk water frequency at 0 ppm. The scan parameters include the following: number of scans = 1, $\pi/2$ pulse = 10 μs, TE = 2 ms, TR = 8 s + T_{sat}, dwell = 60 μs, presaturation amplitude = 1.8 μT. CEST imaging experiments used the RARE fast spin–echo imaging sequence with an magnetization transfer presaturation block pulse. The imaging parameters include the following: slice thickness = 0.5 mm, field of view = 1.4 cm × 1.4 cm, matrix size = 64, RARE factor = 8, $\pi/2$ pulse = 1 ms, echo time = 3.4 ms, repetition time = 10 s, presaturation amplitude = 1.8 μT, $\Delta\omega = 1$ ppm.

4. MTR_{asy} and Exchange Rate Measurements. Since the intraliposomal water peak is close to the bulk water peak, an asymmetry analysis was carried out to subtract out the direct saturation of the bulk water:

$$\mathrm{MTR}_{\mathrm{asy}}(\Delta\omega) = \frac{M_{\mathrm{sat}}(-\Delta\omega) - M_{\mathrm{sat}}(\Delta\omega)}{M_0} \approx \mathrm{PTR}(\Delta\omega) \tag{10}$$

These asymmetry spectra remove much of the effect of direct water saturation. We determined the exchange rate of water across the liposomal membrane based on the increase in MTR_{asy} as a function of presaturation time (T_{sat}), as expressed in eq 5 (termed "QUEST" by McMahon et al.[26]). The relaxation times of phosphate buffered saline (denoted "w,0") and 200 mM TmDOTA (denoted "*l*") were experimentally determined using inversion–recovery and single spin–echo sequences at 11.7 T: $T_{1w,0} = 2.98$ s, $T_{2w,0} = 0.93$ s, $T_{1l} = 28.2$ ms, $T_{2l} = 16.6$ ms. These empirical values were used directly in all the model analyses. Since MTR_{asy} depends on the presaturation pulse frequency ($\Delta\omega$), in principle, it should be measured for all positive frequencies and integrated to obtain a frequency-independent quantity. This quantity can then be used to evaluate for a set of T_{sat} measurements. Here we simplify the measurements by using only the maximum of the MTR_{asy} peak at $\Delta\omega = 1$ ppm, assuming that the widths of the MTR_{asy} peaks do not vary significantly for the different T_{sat} durations for a given sample.

Three methods were used to determine the exchange rate from MTR_{asy} versus T_{sat}. The output parameters are the exchange rate k_{wl}, the longitudinal relaxation time T_{1w}, and the saturation efficiency α. Method (i) uses eqs 5 and 6 to fit for k_{wl} and α, then obtains T_{1w} from the fitted value of k_{wl}; method (ii) uses eqs 5 and 7 to fit for k_{wl} and T_{1w}, then obtains α from these fitted values; method (iii) numerically solves the Bloch equations of a two-spin system undergoing exchange and fits for k_{wl} and T_{1w}, then obtains α from these fitted values. Method (i) is the simplest to implement and analyzes each set of liposome data individually to yield one set of (k_{wl}, T_{1w}, α) values. Methods (ii) and (iii) are more involved in

(23) Zou, C. S.; Mahmood, A.; Sherry, A. D. *J. Magn. Reson.* **2001**, *151*, 101–106.
(24) Castile, J. D.; Taylor, K. M. G. *Int. J. Pharm.* **1999**, *188*, 87–95.
(25) Williamson, D. C.; Narvainen, J.; Hubbard, P. L.; Kauppinen, R. A.; Morris, G. A. *J. Magn. Reson.* **2006**, *183*, 215–224.
(26) McMahon, M. T.; Gilad, A. A.; Zhou, J.; Sun, P. Z.; Bulte, J. W. M.; van Zijl, P. C. M. *Magn. Reson. Med.* **2006**, *55*, 836–847.

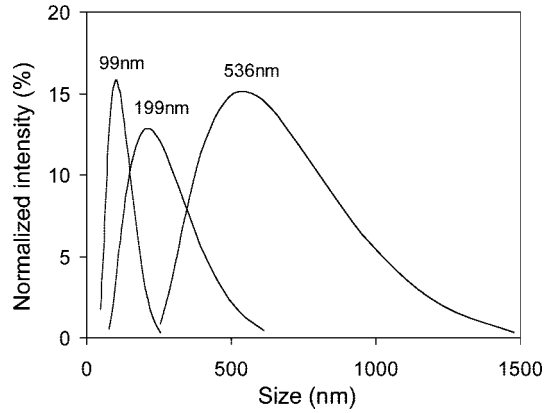

Figure 1. Size distributions of three liposome samples measured from dynamic light scattering.

Table 1. Properties of Liposome in PBS (22 ± 1 °C)

diameter (nm)	[liposome] (nM)	x_l	$\Sigma S/V$ (μm^{-1})	MTR_{asy} @ 1 ppm
99 ± 38	58	0.46%	0.92	0.55
199 ± 101	6.7	0.46%	0.38	0.41
536 ± 224	0.10	0.46%	0.093	0.095

Table 2. Exchange Rate Analysis of MTR_{asy} versus T_{sat} for Three Liposome Samples Using Three Different Methods Outlined in the Experimental Section

method	sample	$\overline{k_{lw}}$ (s^{-1})	k_{wl} (s^{-1})	α	T_{1w} [a] (s)	P_l [b] (μm/s)
(i)	99 nm	194	0.89	0.85	2.11	
	199 nm	94	0.43	0.84	2.20	0.99 ± 0.21
	536 nm	12	0.056	0.84	2.65	
(ii)	99 nm	174	0.80	0.93		
	199 nm	88	0.40	0.95	1.85	0.89 ± 0.21
	536 nm	13	0.062	0.99		
(iii)	99 nm	221	1.02	0.88		
	199 nm	93	0.43	0.95	2.03	1.11 ± 0.14
	536 nm	13	0.059	0.99		

[a] T_{1w} is calculated for each sample in method (i); it is treated as a single fit parameter in methods (ii) and (iii). [b] Errors in permeability are 95% confidence intervals in the linear coefficients of exchange rates versus $\Sigma S/V$.

implementation: three sets of liposome data corresponding to three different size distributions are analyzed together in a multivariate fit to yield three sets of (k_{wl}, T_{1w}, α) values simultaneously. The intraliposomal water fraction and TmDOTA concentrations were adjusted to the same value for all samples, thus the bulk TmDOTA concentration remained constant. As a result, T_{1w} is expected to be the same and is treated as a single fit parameter for all samples in methods (ii) and (iii) (Table 2). Finally, the permeability was obtained from linear regression analysis of k_{wl} versus total surface-to-volume ratio using eq 4.

IV. Results and Discussion

The hydrodynamic size distributions of the three liposome samples are shown in Figure 1. The distributions are monomodal and become broader as the size increases. The distributions are asymmetric favoring particles with larger diameters, which is a typical result of the extrusion process.[27] In Table 1, the *z*-average diameter and the standard deviation of one representative size distribution are reported. The size distributions are highly reproducible for each of the samples, as demonstrated in the consistent *z*-average values for three consecutive measurements on each sample (Supporting Information). To isolate the effect of size on MTR_{asy}, we adjusted the concentrations such that x_l was kept constant at 0.46%.

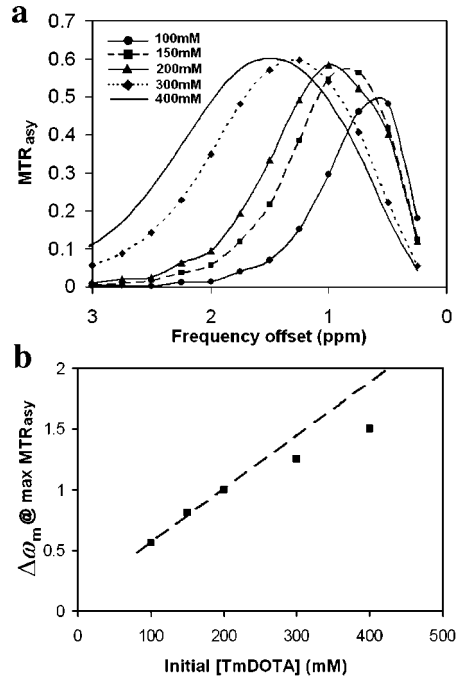

Figure 2. (a) MTR_{asy} versus frequency offset of the presaturation pulse for five liposome samples (diameter ~ 80 nm), each encapsulating a different concentration of TmDOTA from 100 to 400 mM. (b) The frequency offset, $\Delta\omega_m$, at which MTR_{asy} maximizes as a function of the initial TmDOTA concentration. The dashed line represents a linear fit to the three samples with the lowest initial [TmDOTA].

High-resolution proton spectra of the three liposome sizes (Supporting Information), each encapsulating 200 mM TmDOTA, show a small shoulder around 0.3 ppm downfield from the bulk water due to the intraliposomal water. The position of the small shoulder is consistent for all sizes, indicating that the encapsulated TmDOTA concentration is the same for all sizes. The fact that this resonance can be measured separately from the bulk water suggests that the membrane water exchange rate is in the slow exchange regime on the NMR time scale. This is further confirmed by comparing the measured membrane exchange rates in Table 2 (method (iii), $\overline{k_{lw}}$ = 13–221 s^{-1}) with the chemical shift difference (0.3 ppm = 942 rad/s). We see that all the exchange rates indeed fall under the slow exchange regime.

In principle, the intraliposomal water fraction can be estimated from the ratio of the intra- to extraliposomal water peaks on the NMR spectra. However, the intraliposomal peak is too small to be useful for this estimation. Thus, we rely on the fluorescence and DLS measurements to determine the intraliposomal water fraction.

To optimize the entrapped TmDOTA concentrations, we systematically varied the initial TmDOTA concentrations from 100 to 400 mM and produced liposomes of similar sizes (80 nm) using the 50 nm extrusion filters (Figure 2). To better delineate the intraliposomal water signal, MTR_{asy} spectra were used instead of NMR proton spectra. Since the chemical shift of the intraliposomal water is independent of the liposome concentration, the different liposome samples were used directly from the preparation and no further concentrating/diluting was

(27) Berger, N.; Sachse, A.; Bender, J.; Schubert, R.; Brandl, M. *Int. J. Pharm.* **2001**, *223*, 55–68.

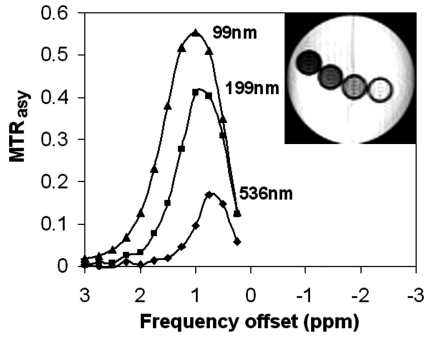

Figure 3. MTR_{asy} versus presaturation frequency offset for three liposome samples of different sizes, each containing 200 mM TmDOTA. Inset is a CEST image of the three samples and PBS buffer: from left to right, 99 nm, 199 nm, 536 nm, buffer.

required. Increasing TmDOTA concentrations from 100 to 400 mM shifts the MTR_{asy} curves toward low field from 0.5 to 1.5 ppm. To show the correlation between the MTR_{asy} curve shift and the TmDOTA concentrations, the chemical shift at the maximum $MTR_{asy}(\Delta\omega_m)$ of each curve is plotted against the initial TmDOTA concentrations (Figure 2b). The $\Delta\omega_m$ was read from the spline curve fit of the data. The MTR_{asy} peak shifts linearly with the TmDOTA concentration up to 200 mM, then begins to deviate from linearity, indicating a "crowding" effect whereby the actual [TmDOTA] inside liposomes was in fact less than the initial $[TmDOTA]_0$. In addition, the maximum MTR_{asy} plateaus (Figure 2b) at 60% near 200 mM $[TmDOTA]_0$, which we attribute to the bulk water T_2 line broadening due to the presence of the Tm(III) ions. For example, the direct saturation as indicated by the saturated water signal at the opposite frequency side of water (0 ppm) was 7% for the 100 mM $[TmDOTA]_0$ sample and rose to 27% for the 400 mM $[TmDOTA]_0$ sample. Taking into consideration both maximizing MTR_{asy} and minimizing $[TmDOTA]_0$, we chose 200 mM as the optimum bulk TmDOTA concentration for the size-dependent studies. Since the smallest liposome size was used in this investigation, the crowding effect should not be a problem for the other two larger liposome sizes. All subsequent liposome size measurements were carried out using 200 mM $[TmDOTA]_0$.

Figure 3 shows MTR_{asy} versus frequency offset for the three liposome samples at the 200 mM initial TmDOTA concentration. The spectra show that the CEST effect increases with reduced liposome size, consistent with our theoretical predictions (eqs 2–5). A 5-fold reduction in size from 536 to 99 nm produces an almost 6-fold enhancement in MTR_{asy} (Table 1). This size effect is further confirmed by CEST imaging (Figure 4, inset) in that the smallest liposome size also appears the darkest.

To understand the mechanism for the size-dependent CEST effect in liposomes, membrane water exchange rates were determined from MTR_{asy} for various durations of the presaturation pulse (Figure 4). The fit results are summarized in Table 2. Each of the three analysis methods has pros and cons. Method (i) is the simplest to implement and provides a good estimation of the exchange rate values, but it underestimates the saturation efficiencies. Method (iii) solves the Bloch equations numerically and provides a complete solution but is cumbersome to implement and requires expert NMR background. Method (ii) is an intermediate and practical approach in terms of implementation and accuracy of the fitted exchange rate values, as long as the exchange rate is not too large ($k < \sim 150$ Hz).[26] Although these methods differ in the choice of fit parameters, the exchange rates and T_{1w} obtained are quite consistent, demonstrating the robustness of all three methods.

The accuracies and limitations of methods (i) and (ii) can be judged by comparison to method (iii) because method (iii) uses the exact numerical solutions of the Bloch equations. Method (i) is the most empirical of all three and yields satisfactory exchange rates with 88% (99 nm), 99% (199 nm), and 92% (536 nm) accuracies. The inaccuracy may be the result of assuming that the large difference in MTR_{asy} between the smallest and largest liposomes can be accounted for by the difference in their saturation efficiencies. However, this assumption is unwarranted because, while the measured MTR_{asy} decreased by almost 6-fold in going from the smallest to the largest liposomes, α increased by only 1.1-fold according to method (iii). Another source of inaccuracy may come from the errors in the calculated values of T_{1w} due to the experimental errors in the measured relaxation times.

Method (ii) is relatively straightforward to implement and does a surprisingly good job in predicting both the saturation efficiencies and exchange rates. Given that the intraliposomal water peak is only around 1 ppm away from the bulk water peak, we would expect some overlap between the presaturation RF pulse and the bulk water peak. The proximity of the two peaks violates one of the assumptions involved in the derivation of eq 5. However, fitting the MTR_{asy} data with eq 5 yields accurate α values for all samples as compared to method (iii). The accuracies of the exchange rates are 79% (99 nm), 95% (199 nm), and 100% (536 nm). One reason for the robustness of this analytic model is likely due to the usage of MTR_{asy} in eq 10 as opposed to just $MTR(\Delta\omega)$. By subtracting the direct saturation contribution from the opposite side of the bulk water peak, the resulting MTR_{asy} more accurately captures the true PTR in the absence of direct saturation described in eq 5.

An important distinction between method (i) and the other two is that the longitudinal relaxation of water (T_{1w}) in the presence of paramagnetic agents is calculated in the former but is allowed to freely vary in the latter two. T_{1w} is crucial to the CEST effect because it determines the total time a labeled water spin can stay saturated. The longer the T_{1w}, the more labeled spins can accumulate and the stronger the CEST signal. Thus, T_{1w} influences both the steady-state MTR_{asy} and the rate at which MTR_{asy} can reach this steady-state value over a prolonged saturation and should be determined accurately to yield a reliable exchange rate. We find that the range of analytical T_{1w} from method (i), 2.11–2.65 s, agrees well with the fitted T_{1w} (2.03 s) from method (iii). Given that the measured T_1 of the buffer solution is $T_{1w,0} = 2.98$ s, our analysis implies that the presence of TmDOTA at 200 mM intraliposomal concentration, or 0.9 mM bulk concentration, shortens this T_1 by 32%.

The exchange rates increase dramatically by 17-fold for a 5-fold reduction in liposome sizes (method (iii), Table 2), in agreement with the increase in the total surface-to-volume ratio ($\Sigma S/V$). The ratio between exchange rate and $\Sigma S/V$ is the membrane permeability (eq 4). Figure 4d shows the linear fits of the exchanges rates from the three methods plotted against $\Sigma S/V$, and the results are summarized in Table 2. The average permeability from method (iii) is 1.11 ± 0.14 μm/s. Individually, the small and medium liposome samples yield the same permeability of 1.1 μm/s; however, the large liposome sample gives a somewhat lower permeability of 0.63 μm/s and contributes to the large standard deviation. A similar trend is seen in the results from the other two methods. Permeability is an intrinsic physical property of the membrane composition and

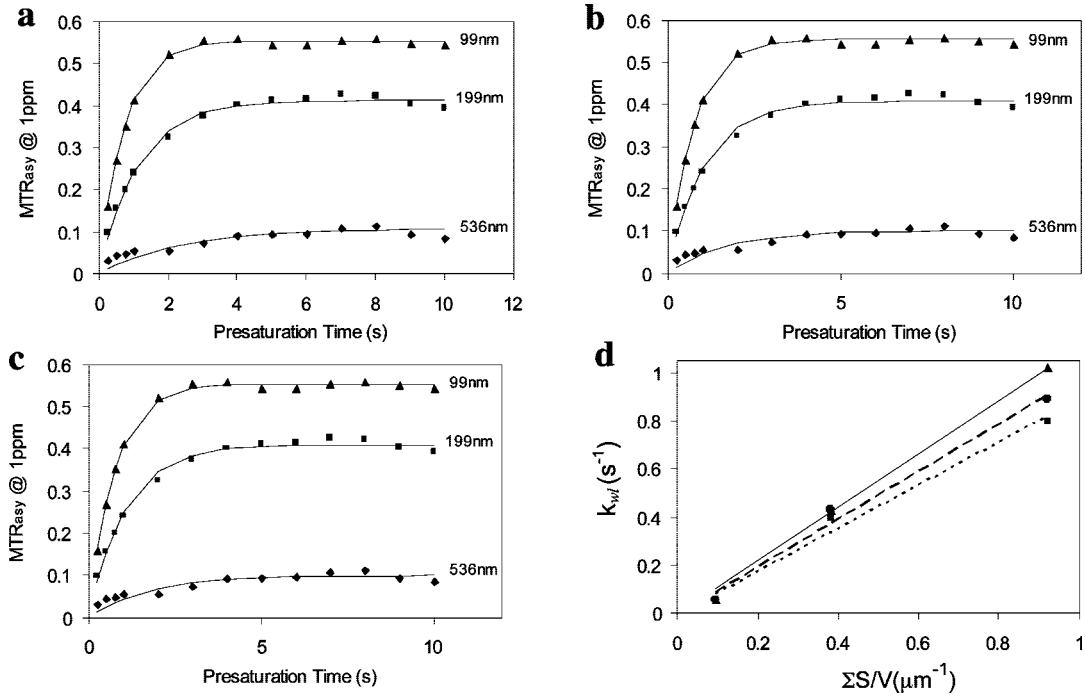

Figure 4. MTR_{asy} at 1 ppm measured with respect to the presaturation time T_{sat} for the three liposome sizes each containing 200 mM TmDOTA. The data are analyzed by three methods: (a) method (i), using eqs 5 and 6 to fit for k_{wl} and α and obtaining T_{1w} from the fitted value of k_{wl}; (b) method (ii), using eqs 5 and 7 to fit for k_{wl} and T_{1w} and obtaining α from these fitted values; (c) method (iii), fitting for k_{wl} and T_{1w} by numerically solving Bloch equations and obtaining α from these fitted values. (d) Linear regression analyses of the exchange rates from method (i) (●, dashed line), method (ii) (■, dotted line), method (iii) (▲, solid line) versus the total surface areas per volume. The slope represents the permeability of liposomal membrane according to eq 4.

should not have a large dependence on the liposome size. The low permeability observed in large liposomes may be due to the inaccuracy of DLS size determination for micron-sized particles and large liposomes settling down during the MR measurements. Another possibility could be related to the packing of the lipid bilayer. Larger liposomes have less curvature and a more closely packed lipid architecture and thus are expected to have a reduced membrane permeability to water.

Since the water permeability of liposome membrane sensitively depends on lipid composition and temperature, a comparison with literature permeability values must take these parameters into account. Koenig et al.[22] constructed liposomes with a different lipid, 1-palmitoyl-2-oleoyl-phosphatidylcholine (POPC), at different molar ratios of POPC/cholesterol from 100 to 60%. They analyzed the nuclear magnetic relaxation dispersion (NMRD) profiles of liposomes encapsulating $Gd(DTPA)^{2-}$ and calculated the permeability based on the measured T_1. Their lipid composition of 60% POPC and 40% cholesterol at 25 °C (cf. our composition of 50% egg PC and 50% cholesterol at 22 °C) yielded a permeability of 8.7 μm/s. Cholesterol tends to stabilize the packing of the long carbon chains and decrease phospholipid mobility, thus lowering the water permeability. So it is expected that the higher cholesterol level at a lower temperature in our study will give rise to a lower permeability value.

A physical picture for the size dependence of the CEST contrast emerges from the above analysis. A small liposome sample with an intraliposomal water volume equal to that of a large liposome sample has more total surface areas because the surface-to-volume ratio is higher for small liposomes (Table 1). More surface area allows more efficient exchange of water across the membrane, thus enhancing the labeling of bulk water surrounding the labeled intraliposomal water (Table 2). This amplification process is repeated for the duration of the presaturation pulse and gives rise to the observed enhanced CEST effect in the small liposomes. Furthermore, since eq 4 still holds and both $\overline{k_{lw}}$ and T_{1w} increase with temperature, the size-induced enhancement in lipoCEST should also occur at 37 °C.

The MR sensitivity enhancement of lipoCEST is 2-fold: CEST enhances sensitivity by the exchange transfer of water magnetization from the inside to the outside of liposomes; additional enhancement comes from the ability of liposomes to package a high payload of contrast materials, in this case the intraliposomal water. In the discussion of contrast materials, we can evaluate the contrast either on a per-molecule or a per-nanoparticle basis. In this paper, our goal is to present a mechanistic picture of the lipoCEST effect, thus we report the contrast on a molecular basis; that is, we compare the resulting MTR_{asy} of different liposome samples after adjusting their intraliposomal water fraction (x_l) to the same value. For other applications, such as contrast agent or drug delivery, it may be more instructive to know the contrast on a per-nanoparticle basis as the goal may involve correlating the image contrast to the number of nanoparticles delivered.

The lipoCEST approach to determine membrane permeability is more straightforward than the previous approach using T_1 relaxation.[7,22,28,29] T_1 is a phenomenological parameter introduced by the Bloch equations. T_1 of the liposomal system depends on the temperature, the chemical exchange rate, the chemical shift difference between the intra- and extraliposomal compartments, and the encapsulated paramagnetic ion concentrations, thus it is difficult to model accurately using basic

(28) Tilcock, C.; MacDougall, P.; Unger, E.; Cardenas, D.; Fajardo, L. *Biochim. Biophys. Acta* **1992**, *1022*, 181–186.
(29) Fossheim, S. L.; Fahlvik, A. K.; Klaveness, J.; Muller, R. N. *Magn. Reson. Imaging* **1998**, *17*, 83–89.

physical principles. Moreover, the T_1 approach requires using a field cycling relaxometer to measure the NMRD profiles over a range of magnetic fields. The field cycling relaxometer is a specialized instrument usually not available in clinical settings and thus may be difficult to gain access. On the other hand, methods (ii) and (iii) presented above do not require a priori assumptions about T_1. The proton transfer ratio is relatively straightforward to model because it involves only the chemical exchange rate, the saturation efficiency, and the relaxation times, all of which can be measured or fitted. In addition, MTR_{asy} can be measured on a conventional MR scanner and does not require specialized instruments.

The control of liposome size can influence not only the lipoCEST contrast but also the in vivo biodistribution and drug uptake if drug molecules are encapsulated. A number of studies have shown that the maximum tumor accumulation depends on both liposome size and composition.[30–32] For example, Liu et al. constructed liposomes containing phosphatidylcholine, cholesterol, and a glycolipid GM1, and found that the highest tumor uptake was achieved with a size range between 70 and 200 nm.[30] They suggested that the larger liposomes outside of this size range were cleared out of the circulation by macrophages of the spleen, and the smaller liposomes were cleared by parenchymal cells of the liver. In another study, using liposomes made of egg phosphatidylcholine, dicetyl phosphate, and cholesterol, Uchiyama et al. found the greatest tumor accumulation with liposome size around 100 nm.[31] Thus, the choice of ~100 nm liposome size that maximizes the lipoCEST contrast in our study is also potentially applicable to in vivo applications of tumor imaging and therapy. Ideally, liposomes smaller than 100 nm with the same total intraliposomal volume would produce even stronger contrast; however, these liposomes are quickly cleared out of the blood circulation by the liver, thus reducing their lifetime in the blood and accumulation in the tumor through the leaky neovasculature. Liver and spleen clearance of liposomes can be significantly reduced by coating the liposome surface with polyethylene glycol (PEG). Using liposomes with a size range of 92–123 nm, Allen et al. showed that PEGylation more than doubled the blood circulation half-life of liposomes while maintaining dosage-independent pharmacokinetics in mice.[32] To optimize both the biodistribution and lipoCEST contrast of liposomes in vivo, these results suggest that the optimal liposome size is in the range of 90–200 nm and liposomes should be PEGylated to have the desirable pharmacokinetic properties.

V. Conclusions

The mechanism for the size-dependent lipoCEST effect, as described in eqs 2–5, is that smaller liposomes have a larger surface-to-volume ratio, thus a larger membrane water exchange rate and lipoCEST effect because PTR is proportional to the water exchange rate at a given x_l (eq 5). Nanoparticles constitute a great platform for sensing the cellular environment, for targeting and imaging biological processes, and for local drug delivery. The ability to optimally design the size of such particles and to quantify and optimize their permeability will be beneficial for these efforts.

Several challenges remain in order to apply CEST imaging, in general, and lipoCEST imaging, in particular, to in vivo and clinical applications. First, the agent should be water-soluble and exhibit low cellular toxicity. As such, agents involving sugars,[33] proteins,[34] polypeptides,[12,26,35] and oligonucleotides[13] may be better tolerated by biological systems. Biodegradable nanocapsules such as liposomes could prove to be highly useful for encapsulating and delivering more toxic CEST agents to their targets,[36] in particular, when the goal is to target and kill cancer cells with these substances. Second, the agent should have a long circulation time and be able to cross biological barriers to reach its target. In this regard, conjugation chemistry approaches that have been used for Gd(III) chelate-based imaging applications may be applied to new CEST agents to improve their ability to reach the desired target.[3] Finally, CEST agents whose resonance frequencies are close to water require additional effort in pulse sequence optimization and data analysis. The optimum presaturation pulse power and duration should be determined experimentally to ensure high saturation efficiency of the agent and low direct saturation of the bulk water. Also, shimming and centering of the bulk water frequency are crucial for the MTR_{asy} analysis to work properly in vivo. However, it is likely that many of these challenges can be met and that CEST will develop into an important contrast for MRI.

Acknowledgment. We thank James Ratnakar, Garry Kiefer, Jiangyang Zhang, and Maria Mikhaylova for help with the experiments. This research was funded by grants from the NIH (R21EB005252, K01EB006394, RO1CA115531, PO1DK058398 and P41RR02584) and the Robert A. Welch Foundation (AT-584).

Supporting Information Available: Two tables with dynamic light scattering measurements and optimization of TmDOTA concentrations; one figure of proton NMR spectra; error analysis of the measured permeabilities. This material is available free of charge via the Internet at http://pubs.acs.org.

JA710159Q

(30) Liu, D.; Mori, A.; Huang, L. *Biochim. Biophys. Acta* **1992**, *1104*, 95–101.
(31) Uchiyama, K.; Nagayasu, A.; Yamagiwa, Y.; Nishida, T.; Harashima, H.; Kiwada, H. *Int. J. Pharm.* **1995**, *121*, 195–203.
(32) Allen, T. M.; Hansen, C. *Biochim. Biophys. Acta* **1991**, *1068*, 133–141.
(33) van Zijl, P. C. M.; Jones, C. K.; Ren, J.; Malloy, C. R.; Sherry, A. D. *Proc. Natl. Acad. Sci. U.S.A.* **2007**, *104*, 4359–4364.
(34) Zhou, J.; Lal, B.; Wilson, D. A.; Laterra, J.; van Zijl, P. C. M. *Magn. Reson. Med.* **2003**, *50*, 1120–1126.
(35) Gilad, A. A.; McMahon, M. T.; Walczak, P.; Winnard, P. T.; Raman, V.; van Laarhoven, H. W.; C.M., S.; Bulte, J. W. M.; van Zijl, P. C. *Nat. Biotechnol.* **2007**, *25*, 217–219.
(36) Torchilin, V. P. *Nat. Rev. Drug Discovery* **2005**, *4*, 145–160.